phys. stat. sol. (b) **241**, No. 11, 2516–2528 (2004) / **DOI** 10.1002/pssb.200302045

Structural, electronic and optical calculations of $Cu(In,Ga)Se_2$ ternary chalcopyrites

M. Belhadj, A. Tadjer, B. Abbar[*], **Z. Bousahla, B. Bouhafs,** and **H. Aourag**

Computational Materials Science Laboratory, University of Sidi-Bel-Abbes, Sidi Bel Abbes 22000, Algeria

Received 14 February 2003, revised 11 May 2004, accepted 18 May 2004
Published online 13 July 2004

PACS 61.50.Ah, 61.66.Fn, 71.15.–m, 71.20.Nr, 77.22.Ch, 78.20.Ci

In this work, we have investigated the structural, electronic and optical properties of the ternary I–III–VI_2 chalcopyrite semiconductors ABX_2 (A = Cu, B = In, Ga, X = Se) by means of a first-principles density-functional total-energy calculation with the local-density approximation (LDA), using the all-electron full-potential linear-augmented plane-wave method (FP-LAPW). The equilibrium lattice constants and the bulk moduli (a, c, c/a, u and B_0) are compared with other theoretical calculations. The energy gap at ambient pressure is found to be direct and the nature of the gap crucially depends on the manner in which the d electrons of the A atoms are treated. We have also reported the optical properties of two chalcopyrite semiconductors $CuInSe_2$ and $CuGaSe_2$. Results on complex dielectric functions, refractive indices n, extinction coefficients k, and normal-incidence reflectivity R in the two crystals are given and compared with earlier data where available. We analyze in detail the structures of the dielectric function observed in the studied energy region.

1 Introduction

In this paper we report the calculated equilibrium lattice constants and electronic structure studies of ternary chalcopyrite ABX_2 (A = Cu, B = In, Ga, X = Se) performed at ambient pressure. $CuInSe_2$ and $CuGaSe_2$ possess the tetragonal structure type space group I42d [1], with four formula units per cells, they are considered as mixed crystals where the divalent cations of the zincblende ZB structure have been alternately replaced by monovalent and trivalent cations. The I–III–VI_2 compounds can be regarded as the ternary analogs of the II–VI binary compounds. One can define a binary analog to each ternary compound (ABX_2) by taking the cation that is situated in the periodic table between the A and B atoms. For example, the ZnSe is the binary analog of $CuGaSe_2$ or $Zn_{0.5}Cd_{0.5}Se$ is the binary analog of $CuInSe_2$. Ternary chalcopyrite crystals are currently of technological interest since they show promise for application in the area of visible and infrared light-emitting diodes, infrared detectors, optical parametric oscillators, upconverters, and far-infrared generation [1]. It has been shown that several ternary compounds can be obtained both p- and n-type. For instance, $CuInSe_2$ within the same family has been recently reported as the highest absorbing semiconductor [2] and, a promising material for photovoltaic solar-energy application [3]. It is known that Cu(In,Ga)Se thin-film solar cells have a high potential to become a leading member of the future solar-cell market [4]. The calculations performed in this paper to obtain structural and electronic properties were obtained using the all-electron full-potential linear-augmented plane-wave method (FP-LAPW) and local density approximation (LDA) [5].

The organization of this paper is as follows. Section 2 deals with the crystal structural aspects. Section 3 describes the computational details. Section 4 deals with the results obtained from our structural and

[*] Corresponding author: e-mail: abbarb@yahoo.fr

electronic calculations, like equilibrium volume and bulk moduli and their comparison with the experimental results. Section 5 describes optical properties. Section 6 deals with assignments of optical transitions and, finally, Section 7 gives the conclusions.

2 Crystal structure

The ternary chalcopyrites crystallize in the tetragonal structure type space group I42d. Thus the chalcopyrite structure is a superlattice of the zincblende structure (ZnS) by doubling its unit cube along the z-axis that becomes the c-axis of the chalcopyrite structure. In most real chalcopyrite crystals, the ratio c/a is approximately equal to two, whereas in an ideal chalcopyrite structure the ratio of the unit cell length c to a is equal to two. The tetrahedral coordination implies that the bonding is primary covalent with sp^3 hybrid bonds prevalent, although there is some ionic character because the atoms are different.

I–III–VI_2 compounds can be regarded as the ternary analogs of the II–VI binary compounds with some interesting structural anomalies [6] relative to their binary. First, unlike their binary analogs, the ternary chalcopyrites have two different cations, for example ZnSe and $CuGaSe_2$. Starting from the A atom and translating in the vertical direction through intervals of $c/2$ we find the sequence ABAB…, whereas translating horizontally with an interval of a, we find the sequence AAAA… Secondly, the ratio between the lattice parameters $n = c/2a$ differs from unity by as much as 2%. Thirdly, the anions are displaced from their zincblende sites. This reflects the fact that in binary AX zincblende compounds each cation A has four anions X as nearest neighbors, whereas in a ternary chalcopyrite ABX_2, each cation A and B has four anions X as nearest neighbors, and each anion has two A and B cations as nearest neighbors. As a result, the anion X usually adopts an equilibrium position closer to one pair of cations than to the other, which results in unequal bond lengths $R_{AX} \neq R_{BX}$ (bond alternation). The nearest-neighbor anion–cation bond lengths are given by

$$R_{AX} = a\,[u^2 + (1 + n)^2/16]^{1/2}$$

and

$$R_{BX} = a\,[(u - (1/2))^2 + (1 + n^2)/16]^{1/2}.$$

Hence, the anion displacement $u - 1/4 = (R_{AX}^2 - R_{BX}^2)/a^2$ measures the extent of bond alternation in the system. Table 1 gives the complete experimental data for a, c, c/a, n, and u of the two ternary compounds $CuInSe_2$ and $CuGaSe_2$. The structural anomalies $n - 1$ and $u - 1/4$ relative to the zincblende structure ($n = 1$ and $u = 1/4$) are seen to be significant.

Table 1 Compilation of the structural parameters a and c (lattice constants), u (anion displacement), and c/a (tetragonal deformation) for the ternary $CuInSe_2$ and $CuGaSe_2$ compounds.

compound	a(Å)	c(Å)	c/a	u	ref.
$CuInSe_2$	5.733	11.40	1.988	0.250	present
	5.784	11.616	2.008	0.224	[14]
	5.782	11.620	2.009	0.235	[15]
	5.733	11.550	2.001	0.220	[16]
$CuGaSe_2$	5.542	10.840	1.957	0.260	present
	5.607	10.990	1.960	0.250	[16]
	5.614	11.030	1.965	0.250	[14]
	5.596	11.003	1.966	0.243	[17]

3 Computational details

We performed first-principles calculations for $CuInSe_2$ and $CuGaSe_2$ within a density-functional theory [7] with the local-density approximation (LDA) using the Perdew and Wang exchange-correlation potential [34]. The Kohn–Sham equations were solved with the full-potential linear-augmented plane-wave (FLAPW) technique, using the WIEN97 code that has been developed by Blaha, Schwarz and their collaborators [33]. The FlAPW method is an all-electron technique and can also deal with systems containing rather localized valence electrons, such as transition metals and their compounds. In the present self-consistent calculations, the electrons are paired into groups, namely the "core" electrons whose charge densities are confined within the "muffin-tin" spheres and the "valence" electrons. The core electron states are treated fully relativistically by solving the Dirac equation for the spherical component of the potential. The valence electrons are treated scalar relativistically. The special *k*-point Brillouin-zone integration technique is used to evaluate new charge densities from the calculated FP-LAPW wave functions. The special *k* points are generated using the Monkhost–Pack [8, 9] scheme we have used 4 special *k* points. The muffin-tin sphere radii used in all our calculations are 2.0 Bohr radius for Cu, 2.5 Bohr radius for In, and 2.5 Bohr radius for Se. The FP-LAPW method is a full-potential method; the final results are not dependent on the muffin-tin radii chosen. Inside the muffin-tin spheres, wave functions, charge densities, and potential are expanded in terms of the spherical harmonics. The cut-off angular momentum (L_{max}) is 12 for wave functions and for charge densities (potentials). The number of plane waves is determined by the K_{max} (largest wave vector), K_{max} = 10 a.u. is used for the valence bands, this gives rise to 7431 and 6630 plane waves for $CuInSe_2$ and $CuGaSe_2$, respectively.

4 Results

4.1 Structural properties

The principal results of our total-energy calculations are summarized in Figs. 1, 2, 3, and 4 where the total energy is shown as a function of unit-cell volume and *c*/*a* ratio. The total energies are calculated in the chalcopyrite structure by changing systematically the volume V_0 and c_0/a_0, where V_0 and c_0/a_0 represent the equilibrium volume and equilibrium lattice constants. The two first curves are Murnaghan's [10] equation of state fitted to the calculated total energies for each compound. The bulk moduli B_0, equilibrium lattice constants (*a*, *c*, *a*/*c*) and anion displacement (*u*) are obtained from these curves. We started our calculations with the preliminary experimental structure parameters. First, we plotted the total energy as a function of the unit-cell volume and fitting the calculated values to the Murnaghan's equation of state (EOSs), where the minimum energy volume is determined. Secondly, we plotted the total energy as

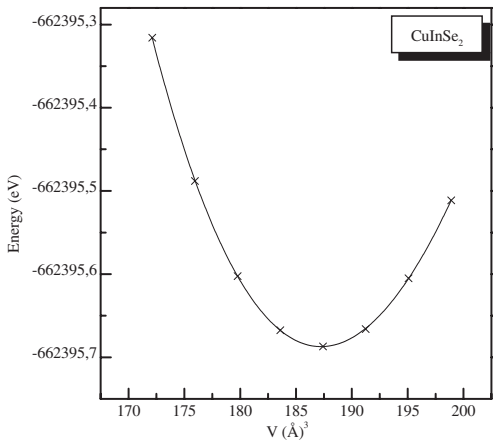

Fig. 1 Variation of total energy (in eV) with volume in $CuInSe_2$.

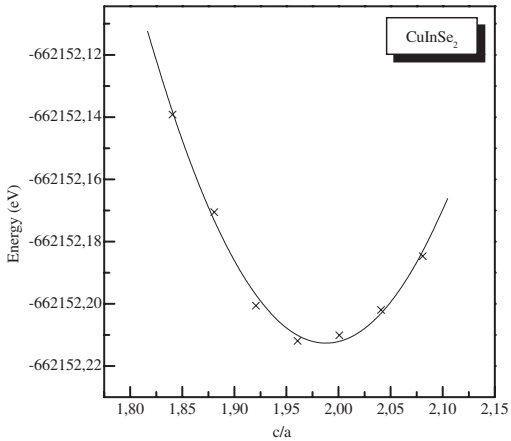

Fig. 2 Variation of total energy (in eV) with ratio *c*/*a* in $CuInSe_2$.

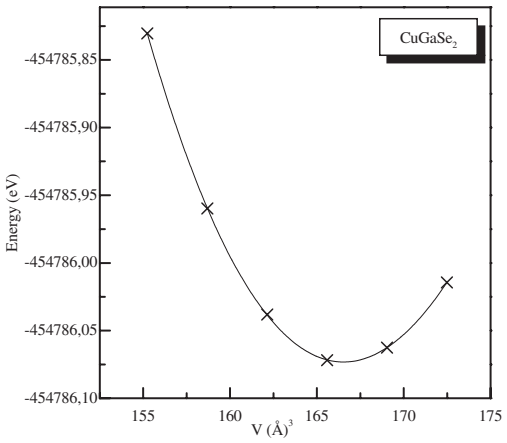

Fig. 3 Variation of total energy (in eV) with volume in $CuGaSe_2$.

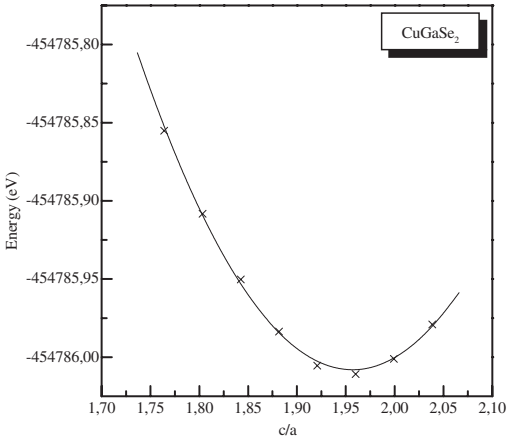

Fig. 4 Variation of total energy (in eV) with ratio *c*/*a* in $CuGaSe_2$.

a function of ratio *c*/*a* and fitting the calculated values to the polynomial equation and determined the minimum *c*/*a*. Thirdly, using the minimum volume and the minimum ratio *c*/*a* we found the final structural parameters of equilibrium (*a*, *c*, and *c*/*a*). Finally, the anion displacement *u* is obtained using the final structural parameters of equilibrium (*a* and *c*),

$$u = 0.5 - (c^2/32a^2 - 1/16)^{1/2}.$$

The calculated values of the structural parameters of the two considered compounds $CuInSe_2$ and $CuGaSe_2$ are shown in Tables 1 and 2 compared with other available theoretical results and experimental data.

5 Electronic properties

5.1 Band structure

Here we describe the energy band structure and the electronic charge distribution in $CuInSe_2$ and $CuGaSe_2$, the simplest ternary analogs of II–VI zincblende compounds. The uppermost valence bands of an I–II–VI_2 compound are profoundly influenced by the proximity of noble metal d-levels in the valence band. The presence of the noble metal d-levels in the valence band has been confirmed directly by the observation of electroreflectance structure due to transitions from the d-levels themselves to the lowest conduction band minimum.

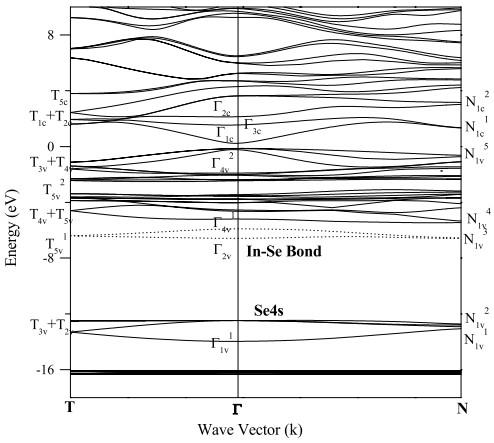

Fig. 5 Electronic band structure of $CuInSe_2$.

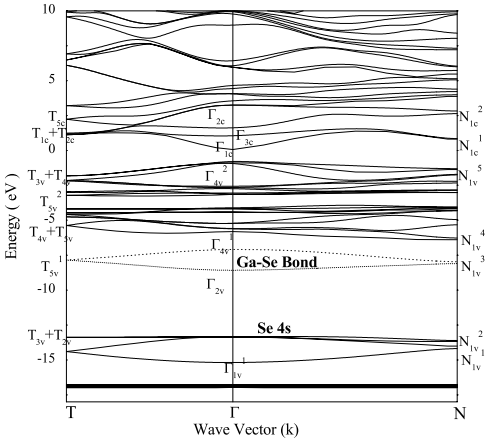

Fig. 6 Electronic band structure of $CuGaSe_2$.

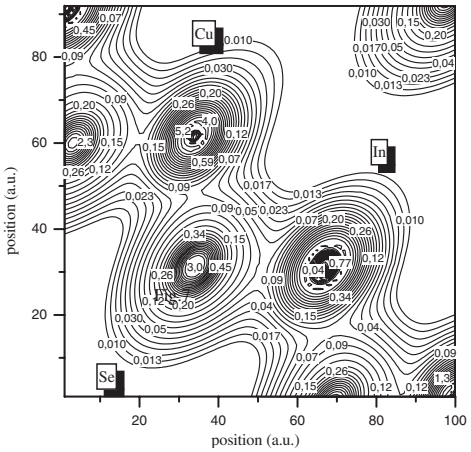

Fig. 7 Total valence charge density in the (110) plane of $CuInSe_2$.

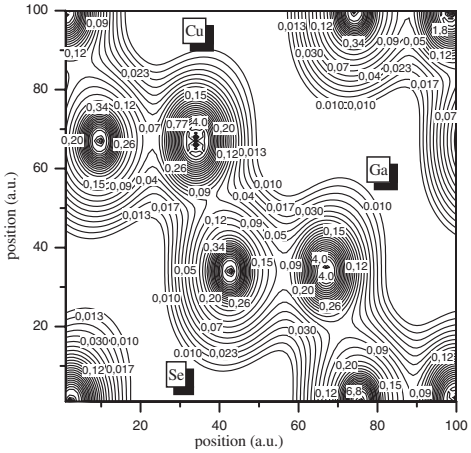

Fig. 8 Total valence charge density in the (110) plane of $CuGaSe_2$.

From the electroreflectance spectrum of $CuGaSe_2$ (Shay et al. [11]), the lowest band gap (1.68 eV) is 1 eV below that of ZnSe, the binary analog, and the spin-orbit parameter of 0.23 eV is considerably less than the spin-orbit splitting measured in ZnSe (0.43 eV). Similar results are obtained for $CuInSe_2$ (Shay et al. [12]), the energy gap is –1.3 eV less than the energy gap in the binary analog $Zn_{0.5}Cd_{0.5}$ Se, and the spin-orbit parameter of 0.23 eV is considerably less than the spin-orbit splitting measured in CdSe (0.42 eV). These two anomalies, the downshift of the energy gaps relative to the binary analogs, and reduced spin-orbit splitting, have been observed to various degrees in all I–II–VI_2 compounds investigated. Shay and Kasper [13] have pointed out that the anomalous reduction in the band gaps of ternary chalcopyrites relative to their binary analogs is correlated with the existence of d bonding in the former compounds. They found that the band gap anomaly ΔE_g correlates nearly linearly with the percentage of *d* character α_d deduced by comparing the spin-orbit splitting of the ternary and binary compound, i.e., $\Delta E_g = a\alpha_d$ with $a \approx 3.125$ eV. They have suggested that $CuInSe_2$ and $CuGaSe_2$ have a nearly constant percentage of *d* character ($\alpha_d = 0.34$ and 0.36, respectively).

In the band-structure calculations, the valence electronic configurations assumed for the atoms of $CuInSe_2$ and $CuGaSe_2$ are given here Cu: $3d^{10}\ 4s^1$, In: $5s^2\ 5p^1$, Ga: $4s^2\ 4p^1$ and Se: $3s^2\ 4p^4$. It should be noted that the d-electrons of Cu are treated as valence electrons (labelled $Cu^+\ 3d^9\ 4s^1$) as it has a direct bearing in deciding the nature of the band gap (direct or indirect). As seen in Figs. 5 and 6, the top of the valence band and the bottom of the conduction band lie along the gamma-point, indicating that these compounds are direct band gap semiconductors. The uppermost valence band is derived from a combination of the p-orbitals of the anion with the d-orbitals of the noble metal, while the conduction band is derived from the s-state of the cation.

The electronic band structure shows a few major subbands below E_F. First, in the region of 0 to –5 eV below the valence-band maximum (VBM), the upper valence band consists of Se p and Cu d states. Secondly, in the energy region $E_{VBM}-6$ to $E_{VBM}-9$ eV, we find the In–Se and Ga–Se band (dashed lines) for the $CuInSe_2$ and $CuGaSe_2$, respectively. Thirdly in the region between $E_{VBM}-12$ to $E_{VBM}-16$ eV, we find the Se 4*s* subband. Finally and above $E_{VBM}-16$ eV, we observe the under-band 4d of the In cation and 3d of the Ga cation for the two compound $CuInSe_2$ and the $CuGaSe_2$, respectively.

The calculated values of the lowest direct band gap of the two considered compounds $CuInSe_2$ and $CuGaSe_2$ are shown in Table 4 compared with other available theoretical results and experimental data.

5.2 Charges densities

Figures 7 and 8 depict the electronic charge density of the valence bands of the $CuInSe_2$ and $CuGaSe_2$. It is seen that the A^I–X^{VI} contact appears covalently bonded with a significant ionic component (i.e., the maximum of charge drawn closer to the X^{VI}). The Cu atom is seen to contribute significantly to the

Table 2 Comparison of experimental and calculated bulk moduli in $CuInSe_2$ and $CuGaSe_2$ compounds in GPa.

compound	B_0 (theory)				B_0 (exp.)
	present	ref. [18]	ref. [19]	ref. [20]	refs. [21, 22]
$CuInSe_2$	53.22	42	64.01	55.8	53.6
$CuGaSe_2$	57.84	46	69.31	68.8	71.0

Table 3 Calculated valence-band and conduction-band energies at high symmetry points (in eV).

state	$CuInSe_2$		$CuGaSe_2$	
	present	ref. [25[a], 25[b]]	present	ref. [25[a], 25[b]]
upper VB				
$\Gamma_{4v}^{(2)}$	0.0	0.0	0.0	0.0
$\Gamma_{5v}^{(2)}$	–0.03976	–0.03	–0.13685	–0.34
$T_{3v} + T_{4v}$	–1.00985	–1.05	–1.05597	–1.14
$N_{1v}^{(5)}$	–0.52211	–0.63	–0.54583	–0.58
low VB				
$\Gamma_{4v}^{(1)}$	–5.07708	–4.66	–5.03915	–4.74
$N_{1v}^{(4)}$	–5.33577	–5.02	–5.62091	–5.21
$T_{4v} + T_{5v}$	–4.48324	–4.61	–4.60281	–4.61
conduction band				
Γ_{1c}	0.25715	0.2	0.83046	0.48
Γ_{3c}	1.64597	1.87	1.79312	1.55
Γ_{2c}	2.24045	2.46	2.36111	2.05
$T_{1c} + T_{2c}$	1.71835	1.64	1.98631	1.63
T_{5c}	2.54896	1.95	2.99582	1.60
$N_{1c}^{(1)}$	1.42172	1.39	1.58227	1.00
$N_{1c}^{(2)}$	3.27202	3.37	3.57922	3.17

Table 4 Calculated lowest direct band gap E_g (in eV).

	$CuInSe_2$	$CuGaSe_2$
E_g^{cal}	0.26	0.83
E_g (ref. [25[b]])	–0.2	0.48
E_g^{expt} (ref. [25[b]])	0.98	1.68

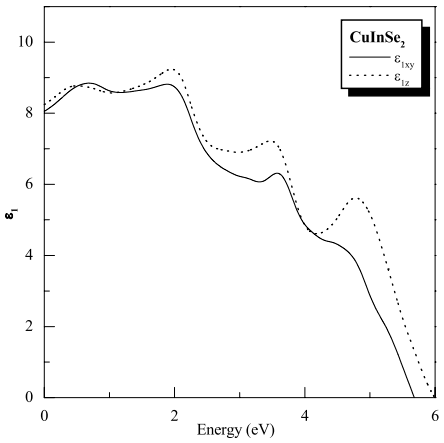

Fig. 9 Ordinary (solid lines) and extraordinary (dashed lines) of real parts of dielectric tensor components of $CuInSe_2$.

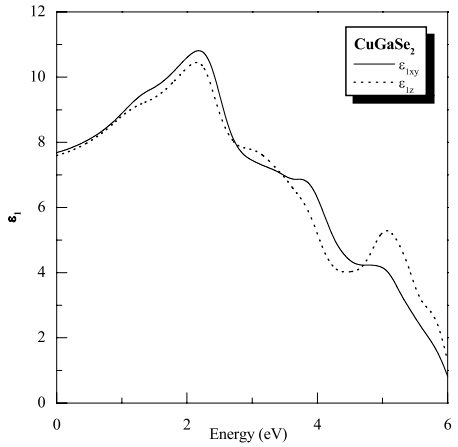

Fig. 10 Ordinary (solid lines) and extraordinary (dashed lines) of real parts of dielectric tensor components of $CuGaSe_2$.

charge in the upper valence band. The bonding in the system is described as a mixed ionic and covalent, where the contours around the Cu–Se contact are shaded to highlight the formation of the bonding.

6 Optical properties

Optical spectra provide extremely useful ways to investigate condensed matter systems. Absorption, reflectivity, photoluminescence and other optical techniques are commonly used to characterize materials. However, the optical properties of ternary chalcopyrite semiconductors provide the basis for a vast range of investigations. In this context, it is important to be able to describe accurately such properties by efficient ab-initio approaches.

6.1 The dielectric function

The most important measurable quantity we address in this section is the dielectric function $\varepsilon(\omega)$ of the system, which is a complex quantity. The optical properties of the two materials are determined by the dielectric function $\varepsilon(\omega)$ given by

$$\varepsilon(\omega) = \varepsilon_1(\omega) + \mathrm{i}\varepsilon_2(\omega) \; .$$

The imaginary part of $\varepsilon(\omega)$, $\varepsilon_2(\omega)$ depends on the joint density of states and the momentum matrix elements. The real part, $\varepsilon_1(\omega)$, was obtained from $\varepsilon_2(\omega)$ by the Kramers–Kronig relations. In Figs. 9–12 we present our calculated imaginary and real part of dielectric function and in Tables 5 and 6 we report the main optical transitions energies (in eV) and their polarization above the fundamental gap. We have performed our calculations using 158 k points in the irreducible Brillouin zone (BZ).

However, the dielectric functions are resolved in two components, $\varepsilon_{2xy}(\omega)$, which is the average of the spectra for ordinary polarization along the x and y directions ($E\perp c$-axis) and $\varepsilon_{2x}(\omega)$ corresponds to the extraordinary polarization along the z-direction ($E//c$-axis). The most important quantity is the zero-frequency limit $\varepsilon(0)$, which is the electronic part of the static dielectric constant that depends strongly on the band gap; using the correction of scissors we have corrected the band gap with 0.72 eV and 0.85 eV for $CuInSe_2$ and $CuGaSe_2$, respectively. This quantity may be related to the refractive index measured at a frequency above the lattice vibrational frequencies. Our calculated static dielectric constant, refractive indices are listed in Table 9. We can note that the general shape of the curves for both compounds is rather similar, indicating the same frequency regions where the $\varepsilon_2(\omega)$ functions are enhanced or de-

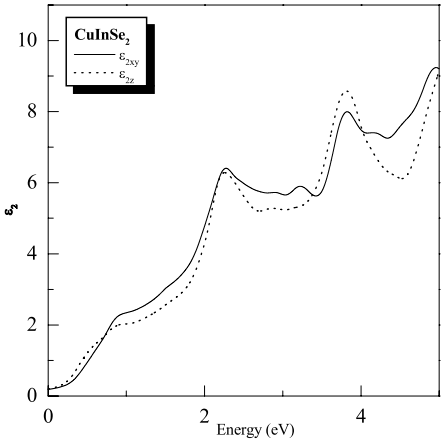

Fig. 11 Ordinary (solid lines) and extraordinary (dashed lines) of imaginary parts of dielectric tensor components of $CuInSe_2$.

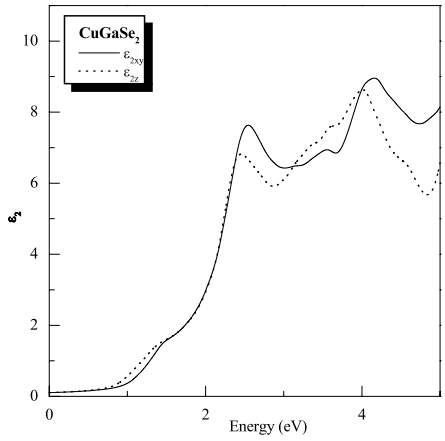

Fig. 12 Ordinary (solid lines) and extraordinary (dashed lines) of imaginary parts of dielectric tensor components of $CuGaSe_2$.

creased from one polarization to another. This, of course, is due to the similarities in their band structures and when interpreting these results, we have remarked that the $CuGaSe_2$ and $CuInSe_2$ spectra have some features in common. First, the calculated $\varepsilon_2(\omega)$ function begins with a transition type-E_0 at Γ, corresponding to the main energy gap, our calculated energy is (0.89 eV and 0.26 for $CuGaSe_2$ and $CuInSe_2$, respectively) are smaller than the experimental gap (1.68 eV and 0.95 eV for both semiconductors, respectively). Secondly, there are three main peaks, the first peak due to transition related to the $N^2_{1v} - N_{1c}$ transition, the second peak due to the transition related to $(T_{3v} + T_{4v})\ [X_{5v}] - T_{5c}[X_{1c}]$ and the last peak due to transition related to $T_{5v}[2X_{5v}] - T_{5c}[X_{1c}]$ for $CuGaSe_2$ and $CuInSe_2$.

Table 5 The principal optical transitions in (eV) for $CuInSe_2$.

label	transition	$CuInSe_2$	
		E//*c*	*E*⊥*c*
E_0(A)	$\Gamma^{(2)}_{4v} \rightarrow \Gamma_{1c}$	0.26 1.04 [26], 1.038 [27]	0.26 1.04 [26], 1.038 [27]
E_0(B)	$\Gamma^{(2)}_{5v} \rightarrow \Gamma_{1c}$		0.30 1.039 [26], 1.042 [27]
$E(\Gamma X)$	$\Gamma^{(2)}_{5v} \rightarrow \Gamma_{3c}$		1.69 2.4 [26], 2.5 [28]
E_1(A)	$N^{(5)}_{1v} \rightarrow N_{1c}$	2.25 2.82 [26], 2.92 [28], 2.92 [29]	2.25 2.901 [26], 2.92 [28], 2.92 [29]
$E(X\Gamma)$	$\Gamma^{(1)}_{5v} \rightarrow \Gamma_{1c}$		2.51 3.17 [26], 3.24 [28]
E_1(B)	$N^{(4)}_{1v} \rightarrow N_{1c}$	2.90 3.635 [26], 3.72 [28], 3.65 [29]	2.90 3.626 [26], 3.72 [28], 3.65 [29]
$E(\Delta X)$	$T_{3v} + T_{4v} \rightarrow T_{1c} + T_{2c}$	3.45 4.07 [26], 4.02 [28], 4.15 [29]	
E_2(A)	$T^{(2)}_{5v} \rightarrow T_{1c} + T_{2c}$		3.78 4.71 [26], 4.85 [28], 4.70 [29]
E_2(B)	$T^{(2)}_{5v} \rightarrow T_{5c}$	3.87 4.84 [26], 4.85 [28], 4.90 [29]	

Table 6 The principal optical transitions in (eV) for $CuGaSe_2$.

label	transition	$CuGaSe_2$	
		E//*c*	*E*⊥*c*
E_0 (A)	$\Gamma_{4v}^{(2)} \rightarrow \Gamma_{1c}$	0.83 1.648 [26], 1.68 [30], 1.686 [31]	0.83 1.648 [26], 1.68 [30], 1.686 [31]
E_0 (B)	$\Gamma_{5v}^{(2)} \rightarrow \Gamma_{1c}$		0.97 1.717 [26], 1.76 [30], 1.760 [31]
$E(\Gamma X)$	$\Gamma_{5v}^{(2)} \rightarrow \Gamma_{3c}$		1.9,2.8 [26]
E_1(A)	$N_{1v}^{(5)} \rightarrow N_{1c}$	2.40 3.127 [26], 3.28 [32], 3.08 [29]	2.51 3.247 [26], 3.28 [32], 3.08 [29]
$E(X\Gamma)$	$\Gamma_{5v}^{(1)} \rightarrow \Gamma_{1c}$		3.12 3.501 [26], 3.35 [32]
E_1(B)	$N_{1v}^{(4)} \rightarrow N_{1c}$	3.58 4.05 [26], 4.20 [32]	3.54 4.03 [26], 4.16 [32]
$E(\Delta X)$	$T_{3v} + T_{4v} \rightarrow T_{1c} + T_{2c}$	3.81 4.49 [26]	
E_2(A)	$T_{5v}^{(2)} \rightarrow T_{1c} + T_{2c}$		4.06 4.89 [26]
E_2(B)	$T_{5v}^{(2)} \rightarrow T_{5c}$	4.11 5.1 [26], 5.0 [29]	

6.2 Refractive index and reflectivity

The refractive indices of ternary chalcopyrite are important optical design parameters, e.g., for distributed Bragg reflectors (DBRs) in vertical-cavity surface-emitting lasers, the complex index of refraction was then obtained from,

$$U = n + \mathrm{i}k = \varepsilon^{1/2} = (\varepsilon_1 + \mathrm{i}\varepsilon_2)^{1/2} ,$$

where n represent the real part of the refractive index and k is the extinction coefficient. Using real and imaginary parts of the dielectric function we can determine the real refractive index n and extinction coefficient k, given by

$$n = [(\varepsilon_1^2 + \varepsilon_2^2)^{1/2} + \varepsilon_1]^{1/2} ,$$

$$n = [(\varepsilon_1^2 + \varepsilon_2^2)^{1/2} - \varepsilon_1]^{1/2} .$$

Our calculated refractive indices and extinction coefficients obtained in both polarizations are listed in Tables 7 and 8.

From the refractive index and extinction coefficients we can derive the normal incidence reflectivity obtained using the equation

$$R = (n-1)^2 + k^2/(n+1)^2 + k^2 = |\mu - 1/\mu + 1|^2 .$$

The normal incidence reflectivity can also give good information of different critical points transitions. In Figs. 13 and 14 we present the curves of the reflectivity calculated in both polarizations.

6.3 Assignment of optical transitions

In the well-known region of the fundamental gap, our calculated transition energies E_0(A) and E_0(B); are gathered in Tables 5 and 6 along with relevant data published before. The transition energies above the fundamental gap obtained from ellipsometry and reflectivity measurements are also collected in Tables 5 and 6. By inspecting all the spectra, we can establish a general pattern for the outstanding optical transitions above the fundamental gap for the $CuGaSe_2$ analyzed in this work.

Table 7 Values of refractive indices n and extinction coefficients k of $CuInSe_2$.

E	$n_\perp$	$n_{//}$	$k_\perp$	$k_{//}$
0.24588	4.09829	4.14364	0.07999	0.10080
0.27309	4.10935	4.15313	0.08804	0.11497
0.38192	4.15279	4.18399	0.14105	0.19662
0.59959	4.21210	4.19907	0.30194	0.34586
0.79004	4.22409	4.18942	0.46298	0.44194
0.98050	4.19511	4.17023	0.55623	0.48613
1.19816	4.18477	4.18181	0.59865	0.51482
1.49745	4.02543	4.23638	0.71571	0.60365
1.71512	4.23622	4.29772	0.80711	0.67930
2.06882	4.31527	4.41203	1.21451	1.11746
2.28648	4.29179	4.26894	1.52559	1.46780
2.50415	4.07934	4.03657	1.49546	1.38813
2.72181	3.93173	3.95886	1.47552	1.31410
2.93948	3.86051	3.94700	1.48802	1.33394
3.18435	3.82010	3.96888	1.53732	1.33784
3.40201	3.80551	4.04910	1.48159	1.41910
3.61968	3.84905	4.14325	1.68826	1.79093
3.83734	3.96335	3.99571	2.05485	2.14389
4.08221	3.76363	3.63326	20.1496	1.96108
4.29988	3.63603	3.55001	20.0175	1.80082
4.51754	3.59431	3.61384	2.11109	1.69136
4.73520	3.61695	3.82431	2.28815	1.85115
5.00728	3.53060	3.96088	2.60411	2.32668

Table 8 Values of refractive indices n and extinction coefficients k of $CuGaSe_2$.

E	$n_\perp$	$n_{//}$	$k_\perp$	$k_{//}$
0.82329	4.13577	4.12353	0.05780	0.07218
0.85050	4.14745	4.13530	0.06066	0.07850
0.95933	4.19761	4.18226	0.07768	0.11688
1.17700	4.30333	4.26195	0.16279	0.22790
1.36745	4.37846	4.31167	0.28596	0.32923
1.55791	4.43385	4.36296	0.37510	0.38370
1.77557	4.52522	4.45647	0.46372	0.46885
1.96603	4.62896	4.56004	0.60357	0.60365
2.18369	4.73816	4.66450	0.80711	0.60465
2.40136	4.73321	4.60249	0.90748	0.93953
2.64623	4.43082	4.31491	1.44915	1.46442
2.86389	4.21013	4.20132	1.56745	1.40627
3.08156	4.41234	4.20504	1.55717	1.50543
3.29922	4.10722	4.17932	1.59978	1.66485
3.51688	4.06960	4.11783	1.69117	1.79235
3.76176	4.10760	4.02977	1.73593	1.94203
3.97942	4.06395	3.92677	2.06864	2.19276
4.19708	3.83578	3.63816	2.25438	2.15005
4.41475	3.67063	3.45772	2.21714	1.97738
4.65962	3.60529	3.40649	2.13879	1.82288
4.87728	3.64201	3.51138	2.16457	1.62885
5.09495	3.66739	3.80703	2.34862	1.98484
5.31261	3.52143	3.81528	2.53384	2.36696

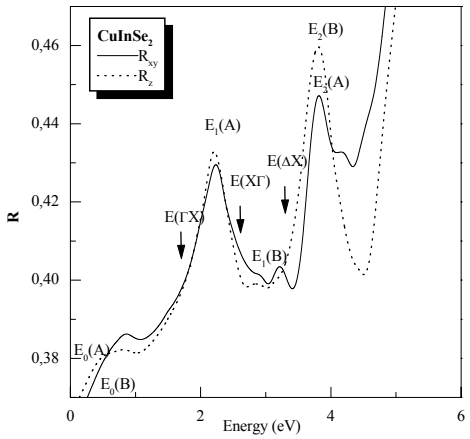

Fig. 13 Polarized reflectivities of $CuInSe_2$ at normal incidence.

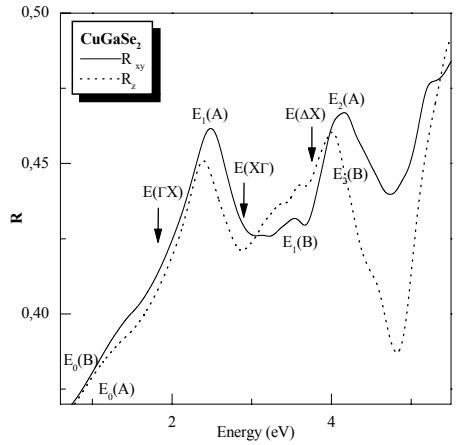

Fig. 14 Polarized reflectivities of $CuGaSe_2$ at normal incidence.

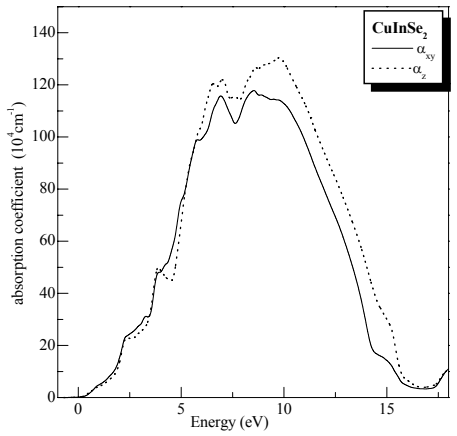

Fig. 15 Absorption coefficient for $CuInSe_2$.

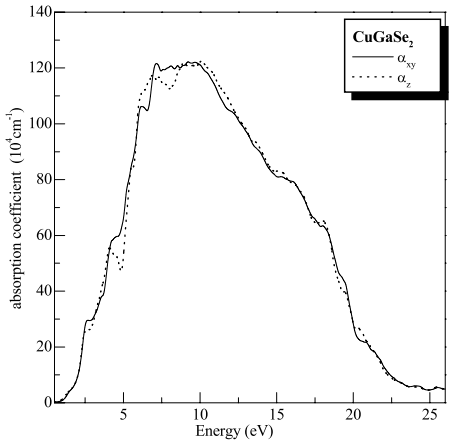

Fig. 16 Absorption coefficient for $CuGaSe_2$.

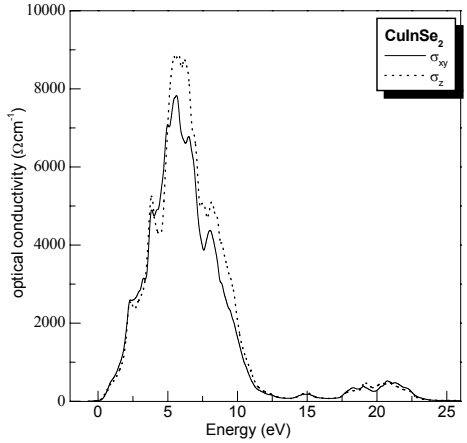

Fig. 17 Optical conductivity for $CuInSe_2$.

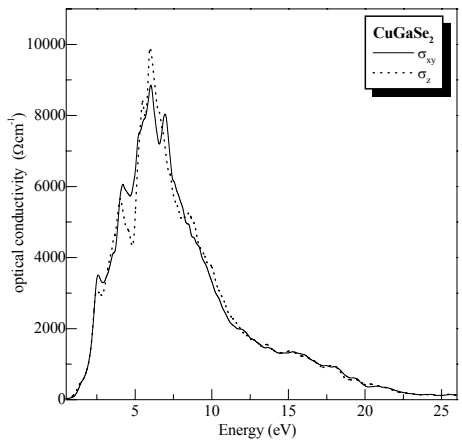

Fig. 18 Optical conductivity for $CuGaSe_2$.

Table 9 The static dielectric function and refractive index for $CuInSe_2$ and $CuGaSe_2$.

compound	$\varepsilon(0)$	$n(0)$
$CuGaSe_2$	8.150	4.037
$CuInSe_2$	7.644	3.910

We associate transitions E_1(A) and E_1(B) to E_1-like transitions at the N point of the Brillouin zone. The assignments of these two transitions E_1(A) and E_1(B) are N^2_{1v} to N_{1c} and N^1_{1v} to N_{1c}, respectively, which appears in both polarizations (perpendicular and parallel). $E(X\Gamma)$ is an interband transition, only allowed in $E \perp c$, with no corresponding direct transition in binary compounds. The three possible assignments by symmetry are the pseudodirect transitions $E(\Gamma X)$: $\Gamma^2_{5v}[\Gamma_{15v}]$ to $\Gamma_{3c}[X_{1c}]$, $E(X\Gamma)$: $\Gamma^1_{5v}[X_{5v}]$ to $\Gamma_{1c}[X_{1c}]$, $E'(\Gamma X)$: $\Gamma^2_{5v}[\Gamma_{15v}]$ to $\Gamma_{2c}[X_{3c}]$. Calculations for our compound predict energies in the sequence $E(\Gamma X) < E_1(A) < E(X\Gamma) < E'(\Gamma X)$. Following this theoretical prediction, we propose to assign $\Gamma^1_{5v}[X_{5v}]$ to $\Gamma_{1c}[X_{1c}]$ to the $E(X\Gamma)$ optical structure. This feature on the high-energy side of E_1(A) corresponds to an interband transition between the heavy-hole p band and the bottom of the conduction band. There is another transition only allowed in $E \perp c$ that we assign to $E'(\Gamma X)$. The structure labelled $E(\Delta X)$ $(T_{3v} + T_{4v})[\Delta_{3v} + \Delta_{4v}]$ to $(T_{1c} + T_{2c})[X_{1c}]$ appears in $E//c$ and has no corresponding direct transition in the binary analogs, it has a matching transition from the upper valence band to the conduction band which would be the pseudodirect transition. Other transitions are observed at the T point of the Brillouin zone E_2(A): $(T_{3v} + T_{4v})[X_{5v}]$ to $T_{5c}[X_{1c}]$ and E_2(B): $T_{5v}[2]$ to $T_{5c}[X_{1c}]$, allowed in perpendicular and parallel polarizations, respectively.

In all spectra the first strong transition above the fundamental gap, called E_1(A) is allowed in both polarizations ($\perp$ and //). At 0.26 and 0.72 eV above there is a weaker transition $E(X\Gamma)$ that appears only in the perpendicular polarization for $CuInSe_2$ and $CuGaSe_2$, respectively. About 0.65 and 1.15 eV above E_1(A) there is another optical transition allowed in both polarizations, labelled E_1(B). Nearby, and only in the parallel polarization, emerges a transition $E(\Delta X)$, located at ≈ 0.55 and 0.26 eV below E_1(B). Close to 4 eV a strong double structure is observed, E_2(A) and E_2(B) are allowed in perpendicular and parallel polarizations, respectively, for $CuInSe_2$ and $CuGaSe_2$, respectively.

6.4 Absorption coefficients and optical conductivity

Our calculations of the absorption coefficients α and optical conductivity for ordinary and extraordinary polarizations are reported in Figs. 15–18. One can notice that very intense absorption due to phonon excitations occurs between 1 eV (λ = 12 400 Å) and 23 eV (λ = 539.1 Å) for $CuGaSe_2$ and between 1 eV (λ = 12 400 Å) and 16 eV (λ = 775 Å) for $CuInSe_2$. We conclude that these compounds can absorb all frequency regions that existed between the UV and IR regions.

7 Conclusion

This paper reports on a study of structural, electronic, and optical calculations of $Cu(In,Ga)Se_2$ ternary chalcopyrites. The ground-state properties, like lattice constants and bulk modulus obtained from our calculations agree very well with other theoretical calculations. One of the most important aspects of these calculations is that it brings out the important role played by the d-state of the noble metals. Furthermore, a recent energy-band calculation that ignored d-bands has predicted $CuInSe_2$ to be an indirect band gap semiconductor, which is a surprising result, since all the I–III–VI_2 compounds that have been studied so far both experimentally and theoretically have proved to have direct band gaps. Their binary analogs also behave as direct band gap semiconductors at ambient pressures. Hence in our calculations, the d-states of the noble metals has been treated as the valence states, which give the correct nature of the energy band gap.

We have also presented the dielectric tensor components of the two ternary chalcopyrites $Cu(In,Ga)Se_2$. Our results for the real and imaginary parts of the dielectric functions are used to repro-

duce optical constants, such as the refractive index, absorption coefficient and optical conductivity. In addition we have given assignments for the most important transitions taking into account band-structure calculations and the appropriate selection rules for coupling between electronic states.

References

[1] J. L. Shay and J. H. Wernick, Ternary Chalcopyrite Semiconductors. Growth, Electronic Properties and Applications (Pergamon Press, Oxford, 1974).
[2] J. E. Jaffe and A. Zunger, Phys. Rev. B **29**, 1982 (1984).
[3] J. E. Jaffe and A. Zunger, Phys. Rev. B **27**, 5176 (1983).
[4] J. Krustok et al., phys. stat. sol. (a) **178**, 805 (2000).
[5] D. J. Singh, Plane waves, pseudopotential and the LAPW method (Kluwer Acad. Publ., Dordrecht, 1994).
[6] J. E. Jaffe and A. Zunger, Phys. Rev. B **28**, 5822 (1983).
[7] P. Hohemberg and W. Kohn, Phys. Rev. B **864**, 136 (1964).
[8] H. J. Monkhost and J. D. Pack, Phys. Rev. B **13**, 5188 (1976).
[9] J. D. Pack and H. J. Monkhost, Phys. Rev. B **16**, 1748 (1971).
[10] F. D. Murnaghan, Proc. Nalt. Acad. Sci. USA **30**, 244 (1944).
[11] J. L. Shay, H. M. Kasper, and L. M. Schivone, Phys. Rev. B **5**, 5003 (1972).
[12] J. L. Shay, H. M. Kasper, and L. M. Schivone, Phys. Rev. B **7**, 4485 (1973).
[13] J. L. Shay and H. M. Kasper, Phys. Rev. Lett. **29**, 1162 (1972).
[14] H. W. Spiess, V. Haeberln, G. Brandt, A. Rauber, and J. Schneider, phys. stat. sol. (b) **62**, 183 (1974).
[15] J. Parkets, R. D. Tomlinson, and J. Hampshire, J. Appl. Cryst. **6**, 414 (1973).
[16] H. Hahn, G. Frank, W. Klingler, A. Meyer, and G. Stroger, Z. Anorg. Chem. **271**, 153 (1953).
[17] S. C. Abrahams and J. L. Bernstein, J. Chem. Phys. **61**, 1140 (1974).
[18] K. J. Bachmann and H. M. Kasper, J. Electron. Mater. **6**, 431 (1977).
[19] R. Asokamani, R. M. Amirthakumari, R. Rita, and C. Ravi, phys. stat. sol. (b) **213**, 349 (1999).
[20] P. Deus and H. A. Schneider, Crystal Res. Technol. **20**, 867 (1985).
[21] H. Neum, phys. stat. sol. (a) **96**, K121 (1986).
[22] H. Neuman, Cryst. Res. Technol. **18**, 665 (1983).
[23] A. Zunger, J. Perdew, and G. Oliver, Solid State Commun. **34**, 933 (1980).
[24] A. Zunger, Phys. Rev. B **21**, 4785 (1980).
[25] (a) J. E. Jaffe and A. Zunger, Phys. Rev. B **28**, 5829 (1983).
(b) J. E. Jaffe and A. Zunger, Phys. Rev. B **28**, 5835 (1983).
[26] M. I. Alonso, K. Wakita, J. Pascual, M. Garriga, and N. Yamamoto, Phys. Rev. B **63**, 075203 (2001).
[27] J. L. Shay, B. Tell, H. M. Kasper, and L. Shiavone, Phys. Rev. B **7**, 4485 (1973).
[28] J. Austinat, H. Nelkowski, and W. Schrittenlacher, Solid State Commun. **37**, 285 (1981).
[29] T. Kawashima, S. Adashi, H. Miyake, and K. Sugiyama, J. Appl. Phys. **84**, 5202 (1998).
[30] J. L. Shay, B. Tell, H. M. Kasper, and L. M. Shiavone, Phys. Rev. B **5**, 5003 (1972).
[31] S. Shirakata, S. Chichibu, and S. Isomura, Jpn. J. Appl. Phys. **17**, 521 (1997).
[32] A. V. Matveev, V. E. Grachev, V. V. Sobolev, and V. E. Tazlavan, phys. stat. sol. (b) **194**, K7 (1996).
[33] P. Blaha, K. Schwartz, and J. Luitz, WIEN97 (Technical University, Vienna, 1997). (Improved and updated unix version of the original copyrighted wien code that was published by P. Blaha, K. Schwartz, P. l. Sorantin, and S. B. Trickey, Comput. Phys. Commun. **59**, 399 (1990)).
[34] J. P. Perdew and Y. Wang, Phys. Rev. B **45**, 13244 (1992).